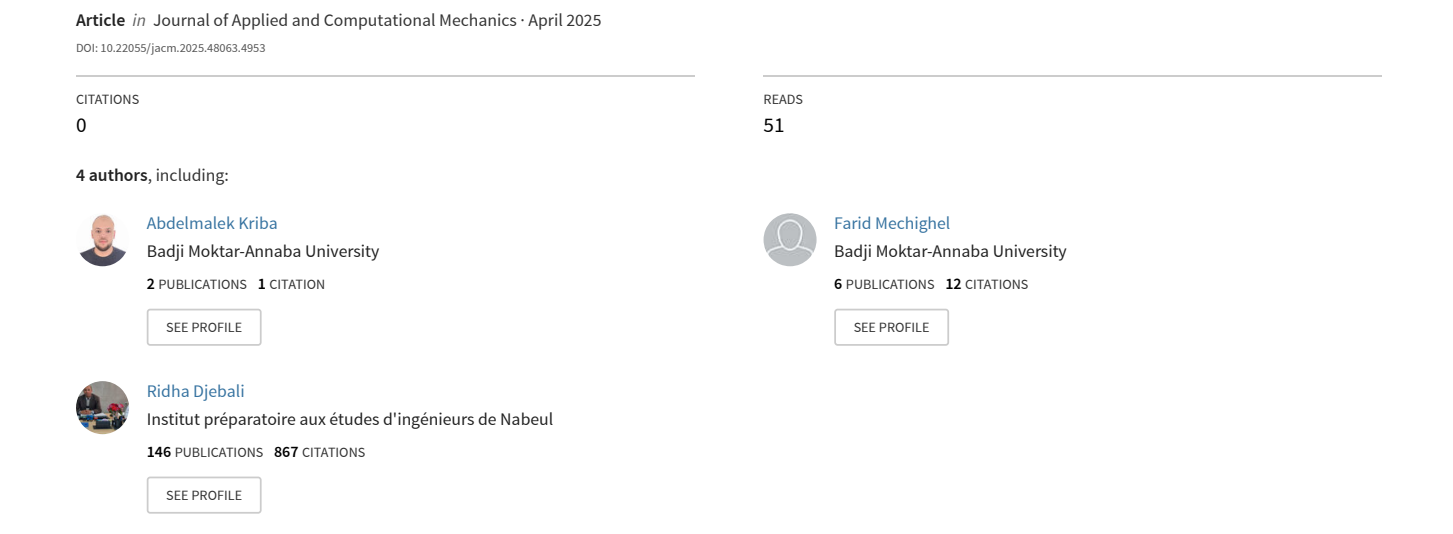
DoE Optimization of Applied Pressure and Mold Size in Manufacturing Homogeneous Alumina Samples by SPS Process under 1000A Current





University of Ahvaz

Journal of

Applied and Computational Mechanics



Research Paper

DoE Optimization of Applied Pressure and Mold Size in Manufacturing Homogeneous Alumina Samples by SPS Process under 1000A Current

Abdelmalek Kriba¹, Farid Mechighel^{1,2}, Ridha Djebali³, Ali J. Chamkha⁴

Received December 03 2024; Revised March 02 2025; Accepted for publication April 12 2025. Corresponding authors: F. Mechighel (farid.mechighel@etu.unilim.fr); R. Djebali (ridha.djebali@ipein.rnu.tn) © 2025 Published by Shahid Chamran University of Ahvaz

Abstract. Spark plasma sintering (SPS) presents advantages over conventional sintering methods, notably high heating rates and reduced residence times. However, SPS suffers from uneven temperature and stress distributions due to suboptimal sintering parameters, such as uniaxial pressure and mold dimensions. These inconsistencies can result in microstructural inhomogeneities, adversely affecting the mechanical properties of the final products. To mitigate these issues, optimizing the sintering parameters is important for achieving a homogeneous polycrystalline material with desired mechanical characteristics. This study focuses on the numerical modeling of the thermoelectric and mechanical coupling behavior of alumina during SPS. Simulations were conducted using ANSYS software, and the model was integrated into a Box-Behnken Design of Experiment (BBD) to optimize three key factors: Factor 1 - uniaxial pressure (5 MPa to 20 MPa), Factor 2 - mold diameter (19 mm to 50 mm), and Factor 3 - mold height (4 mm to 8 mm). The results from the BBD optimization were analyzed using surface diagrams and ANOVA. The optimal SPS parameters identified for producing homogeneous alumina with desired mechanical properties are: uniaxial pressure of 20 MPa, mold height of 8 mm, and mold diameter of 34.5 mm, calculated for a current of 1000 A. This optimization approach effectively enhances the quality of SPS-sintered materials.

 $\textbf{Keywords:} Spark\ plasma\ sintering, Homogeneous\ alumina, Temperature\ and\ stress, Box-Behnken\ design, ANOVA\ and\ optimization.$

1. Introduction

Sintering is a process in which powdered materials (metals or ceramics) are compacted and sintered by application of heat and pressure and the process is carried out at temperatures below the melting points of these materials. Spark Plasma Sintering (SPS) is a single-stage processing technique that combines electric field sintering with uniaxial pressure forming. This technique has many advantages over other conventional techniques (e.g. hot pressing or hot isostatic pressing), such as high heating rate, elimination of sintering aids and short dwell (holding) time, which minimize the grain growth process, leading to materials with improved quality properties [1-4].

Generally, SPS sintering is characterized by inhomogeneities (gradients) in temperature and stress which can eventually produce inhomogeneities in the microstructure of the sample, especially in the case of large samples or near fillet pieces (parts). Therefore, a deeper understanding of these gradients is needed; this can be completed by establishing a numerical model. In addition, numerical simulation will also minimize the number of experimental runs (trials) required to optimize sintering conditions and tooling geometries to produce sintered samples with consistent and improved working properties. In this context, recently, several numerical models have been developed using the finite element method to study the thermoelectric and mechanical behavior of samples sintered by SPS; and the results of these models contributed to the development of the SPS technique [1, 2].

Many research studies have been focused on the study of the thermoelectric and mechanical behavior of samples sintered by SPS sintering. The aim of these studies was to understand the technique by considering all the effects, both primary and secondary, to perfectly control the process and produce parts (product materials) with the desired characteristics. For example, Wang et al. [5] developed a finite element model to simulate thermoelectric and mechanical coupling in SPS sintered samples, studying the influence of the nature (properties) of the sample (material) and the parameters control over the temperature and stress



¹ Mechanics of Materials and Industrial Maintenance Research Laboratory (LR3MI), Mechanical Eng. Dept., Faculty of Technology, Badji Mokhtar University, 12. P.O. Box, 23000 Annaba, Algeria, Email: kriba.abdelmalek@univ-annaba.dz, kriba.abdelmalek@univ-annaba.org

 $^{^2 \ \} Energy \ and \ Pollution \ Laboratory - Mentouri \ Brothers \ University - Constantine, Algeria, Email: farid.mechighel@univ-annaba.dz, farid.mechighel@etu.unilim.fr$

³ UR22ES12: Modeling, Optimization and Augmented Engineering, ISLAIB, University of Jendouba, Beja 9000, Tunisia, Email: ridha.djebali@ipein.rnu.tn

⁴ Faculty of Engineering, Kuwait College of Science and Technology, Doha, Kuwait, Email: a.chamkha@kcst.edu.kw

distributions in the sample. They found that the displacements and stress distributions depend on the nature of the sample and the stress gradients being greater than the thermal gradients. Mechighel et al. [6] performed a numerical study on the effect of key SPS parameters (electric current density and applied pressure) on temperature and stress distributions in copper and alumina samples. They found that the thermal conductivity of the sample influences the temperature distribution in the sample; while the displacements and stress distributions depend on the mechanical properties (mainly Young's modulus and Poisson's ratio) of the sample. Wei et al. [7] developed a finite element model to model the thermoelectric and mechanical coupling in a sample during its SPS sintering. The model is applied to study temperature and stress distributions in functionally graded materials (FGM) based on Ti and TiB materials. The authors found that stresses and stress gradients at the bottom of the sample are significantly greater than at the core of the sample and are positively related to the heating rate. Yushin et al. [8] numerically studied spark plasma sintering of square plates from aluminum oxide (alumina) and tungsten carbide powder. The objective was to determine the temperature and mechanical stress distributions in each sample and in the mold. They found that, for the alumina sample (an electrically non-conductive material), the temperature increased as it moved away from the center of the sample. Diatta et al. [9] developed a thermoelectric and mechanical model of the SPS process to study the evolution of temperature and stress gradients in the alumina powder. Calculations showed that thermally induced stresses are significant, contributing up to two-thirds of the hydrostatic pressure experienced by the powder, which promotes densification. Bodis and Károly [10] studied the fabrication of a functional gradient microstructure of alumina (Al2O3) by SPS. The objective was to determine the relationship between the temperature gradient in the sample and the main operating parameters of the SPS (notably the sintering temperature). They found that asymmetric and high value sintering temperature can increase the temperature difference (gradients) between opposite sides

Other studies have focused on the microstructure and mechanical properties of SPS-sintered mechanical parts as well as the main SPS operating parameters that directly influence the microstructure and mechanical properties of these parts. For example, Borkar and Banerjee [11] studied the effect of SPS operating parameters (pressure and temperature) on the microstructure and mechanical properties of pure nickel. The results indicated that sintering temperature is the determining factor for the microstructure and mechanical properties of SPS-processed pure nickel; while sintering pressure has a limited impact on these properties. An optimal combination of temperature (850°C) and pressure (80 MPa) was identified for a pure nickel SPS exhibiting the desired microstructure and mechanical properties. Oke et al. [12] explored various SPS process parameters such as sintering temperature, dwell time and heating rate to determine the optimum combination to achieve maximum densification and optimum hardness. Their results showed that the hardness, density and microstructure of sintered materials are strongly influenced by the SPS process parameters. Stuer et al. [13] summarized almost a decade of research on SPS sintering and highlighted that a thorough understanding of the mechanisms involved opens new perspectives for future scientific developments and provides a basis for effective knowledge for industrial manufacturing.

However, to fully exploit the advantages of SPS, such as short dwell time and fast densification rate, it is imperative to optimize the sample sintering profile (i.e. mold profile) and the applied pressure to avoid undesirable side effects such as microstructural defects and thermal instabilities. Indeed, these atomic-scale defects induced by applied pressure can play a crucial role in the degradation of many physical properties of the produced ceramic materials as well as in their stability during their subsequent thermal exposures. In the context of SPS process optimization, it is noted that a number of researchers have used the response surface methodology (RSM) based on Box-Behnken design (BBD) to optimize the system outputs under different input factors. For example: Han et al. [14] used the RSM method to identify the optimal SPS parameters, such as sintering temperature, pressure, and dwell time, to obtain the titanium-zirconium-molybdenum/graphite (TZM/graphite) seal with a titanium foil interlayer. Khajelakzay et al. [15] applied the RSM method to optimize the microstructure and mechanical properties of Si3N4-SiC micro/nano-composites during SPS sintering. Journaki et al. [16] used the RSM method to improve the microstructure and coating properties of Cerium oxide/graphene nanoplatelets (CeO2/GNP) composites fabricated by SPS. Further optimization research has used the statistical methods of RMS design of experiments (RSM-DOE) and analysis of variance (ANOVA) to reduce material waste and the number of experimental runs by optimizing the SPS parameters of NieCreZrO2 composites (Oketola et al. [17]) and Inconel 738LC superalloy (Ogunbiyi et al. [18]). On the other hand, Taguchi design of experiments and analysis of variance (ANOVA) statistical methods have also been used for example by Ujah et al. [19] to optimize SPS parameters to develop Al-CNT-Nb nanocomposites for high transmission conductor networks. And by Kumar et al. [20] to determine the importance of sintering parameters for carbon nanotube (CNT) reinforced aluminum composites. Moreover, Ali et al. [21] used the Taguchi method to study the effect of sintering parameters, such as temperature, pressure and dwell time of sintering, on the mechanical and physical properties of Mg-2.5TiB2 composites. It should be noted here that optimization using response surface methodology (RSM) based on Box-Behnken design (BBD) has been widely used not only in the field of SPS sintering but in several engineering fields, see for example references [22-

Spark plasma sintering (SPS) is an advanced process that combines uniaxial pressure and high-intensity pulsed current to densify materials, while significantly reducing cycle time. This process relies on applying a mechanical load using graphite punches, while passing an electric current through the sample and the mold, which generates rapid Joule heating [5, 10]. Optimization of process parameters is important to improve thermal uniformity and minimize internal mechanical stresses.

The uniaxial pressure, ranging from 5 to 20 MPa, was chosen to evaluate its influence on densification and porosity formation. In addition, the mold diameter, ranging from 19 to 50 mm, as well as the height, ranging from 4 to 8 mm, directly influence the current and temperature distribution, thus impacting microstructural homogeneity. These parameter ranges reflect commonly used conditions [2-9], ensuring better reproducibility and reliable extrapolation of numerical results to practical applications.

Numerous studies on spark plasma sintering (SPS) of alumina have been carried out in recent years, highlighting the physical phenomena underlying these applications, thus highlighting the importance of this material in the industry [5, 7-10]. Since SPS sintering encompasses multiphysical phenomena, the optimization of sintering parameters becomes essential to improve the quality of ceramics, by reducing microstructural defects and enhancing their properties.

The precise control of pressure as well as mold dimensions (diameter and height) is important to ensure a homogeneous distribution of temperatures and stresses during the process. The uniaxial pressure has a direct impact on the densification and compactness of the material, promoting better grain cohesion and a reduction in pores. At the same time, the mold dimensions influence the thermal conduction and the electric field distribution, thus affecting the sintering rate and the uniformity of the microstructure [11-14].

This study uses a Box-Behnken (BBD) optimization approach and analysis of variance (ANOVA) to highlight the complex interaction between these parameters and their effect on the final quality of sintered alumina. The results highlight the importance of precise parameter tuning to obtain a homogeneous, dense ceramic with improved mechanical properties. This research contributes to a better understanding of the mechanisms involved in SPS sintering, thus paving the way for more efficient processes for the manufacture of advanced ceramics.



Table 1. This caption is intended for the table and should be centered.

Test #	Applied pressure (MPa)	Mold diameter (mm)	Mold height (mm)
1	5	19	6
2	20	19	6
3	5	50	6
4	20	50	6
5	5	34.5	4
6	20	34.5	4
7	5	34.5	8
8	20	34.5	8
9	12.5	19	4
10	12.5	50	4
11	12.5	19	8
12	12.5	50	8
13	12.5	34.5	6

The present work uses the three-dimensional simulation model developed and presented in the study of Kriba and Mechighel [27]. The model uses ANSYS software for the numerical solution of the equations governing the thermoelectric and mechanical coupling in the sample and in the SPS machine (device) and thus predicts the distributions of the thermal field, the electric current and the stress field in the sample and in the SPS machine. Then, in a second step, we use a design of experiments (RMS-DOE) based on the three-factor Box-Behnken (BBD) optimization method. The aim is to determine the optimal values of the key parameters of the SPS sintering process (in particular the applied pressure and the geometric characterization of the mold size) in order to obtain a polycrystalline solid material with the desired optimal properties from alumina powder.

2. Methods

2.1. General considerations

As previously indicated the present work uses the approach carried out in reference [27] where the model that governs the thermoelectric and mechanical coupling was developed. Based on this "starting" model, we will proceed to optimize the SPS sintering conditions for an alumina sample and to do this, we must resort to the use of the Box-Behnken optimization method [15-20] which allows to obtain a continuous three-factor design at three levels (Fig. 1). The principle of this optimization method is to create a test plan depending on the number of factors and the intervals between them. In this study, we select the factors as follows: Factor 1 - applied pressure in range (5 MPa - 20 MPa), Factor 2 - mold diameter in range (19 mm - 50 mm), and Factor 3 - mold height in range (4 mm - 8 mm).

In the current simulations, we have fixed the value of the electric current applied to the SPS device at (1000 A) for all the tests performed; this is due to the following reasons: the first one lies in the objective of this work which is the optimization of the mechanical condition (applied pressure) to the SPS device during SPS sintering and the optimization of the dimensions (size) of the mold (i.e. sizing of the punch (plunger) and the die of the SPS machine). The second reason is due to the large number of tests to be performed if we optimize four factors (i.e. adding the electric current as an additional factor). The last more plausible reason is that the current of (1000 A) has proven an increased efficiency for SPS sintering of alumina in previous works, for example [5, 20, 27-29], where it is demonstrated that the current of (1000 A) allows to have a rapid densification, a homogeneous microstructure and better mechanical properties of the produced alumina materials.

2.2. Governing equations

The mathematical model presented below is devoted to model the behavior of the thermoelectric and mechanical coupling in the SPS device during the SPS process of a sample (polycrystalline material). In order to simplify the present analysis, the following hypotheses [1, 6, 25, 26] have been made in the model:

- Application of the optimization plan

Using the Box-Behnken optimization method, the test plan can be determined based on the ranges of the above factors as shown in Table 1.

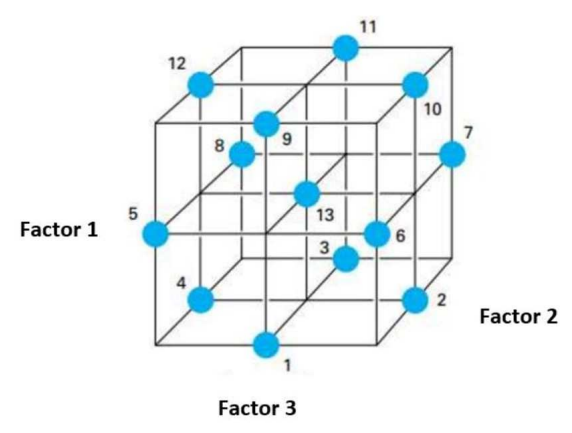


Fig. 1. Box-Behnken design (BBD) for three factors.



As previously stated, we will use the same geometric model of the SPS studied in reference [27] with modifications of the plunger/die/sample geometry imposed by the obtained Box-Behnken design. Figure 2 shows the geometries of the SPS resulting from (corresponding to) all the tests found from the test design by the Box-Behnken method and which will be carried out numerically. The numerical simulations were performed keeping the same mesh element size as in [27] to ensure the reliability of the study, even if the number of nodes and the computation time will be higher, given that the volume of the SPS device increases with the increase in the mold diameter and height (i.e. mold size) imposed by the test design (Fig. 2). Figure 3 shows the exact location of the points (called Point (a) and Point (b)) that we have chosen as reference points to discuss and analyze all the simulation results obtained in all the tests carried out.

3. Results and Discussion

3.1. Thermoelectric behavior

- Electrical behavior

Figure 4 shows the cross-sectional electric current density distributions in the plunger/die/sample system, calculated for all "tested" configurations at the end of the sintering process (at time $t=600\,\mathrm{s}$). Examination of Fig. 4 shows that the general appearance (pattern) of the distribution of the electric current density is almost identical for all the tests carried out. This is due to the electrical boundary conditions imposed on the system which are similar for all test cases. The examination also shows that depending on the dimensions (diameter and height) of the mold and the "applied" pressure, several current density trends can be identified in the plunger/die/sample system and in particular Fig. 4 can be divided into the following three groups of figures.

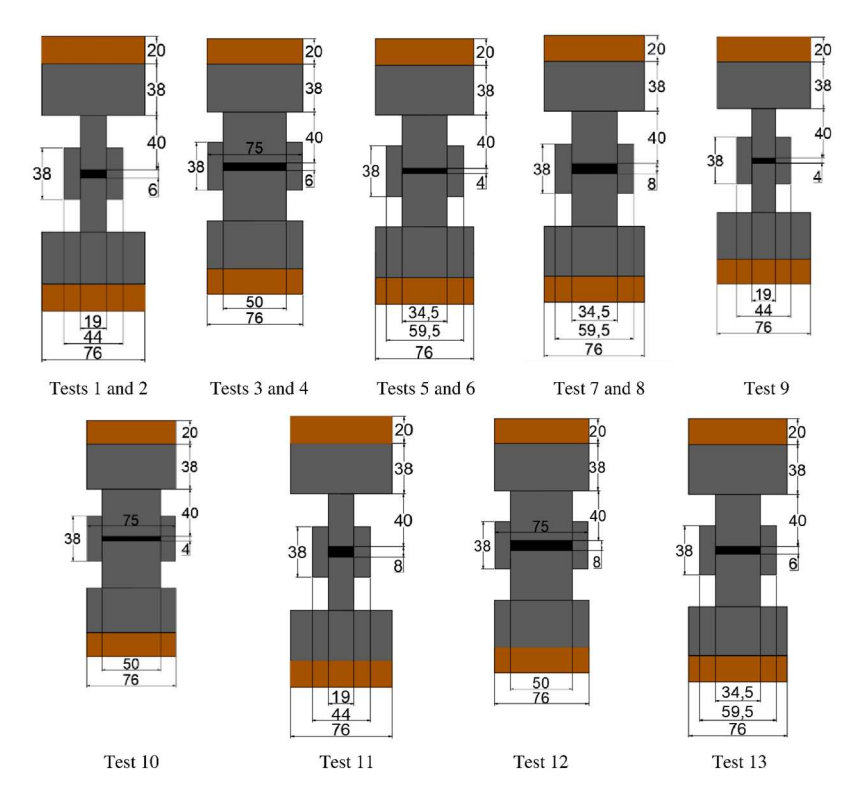


Fig. 2. The different geometries of the SPS resulting from all the tests found from the Box-Behnken method.

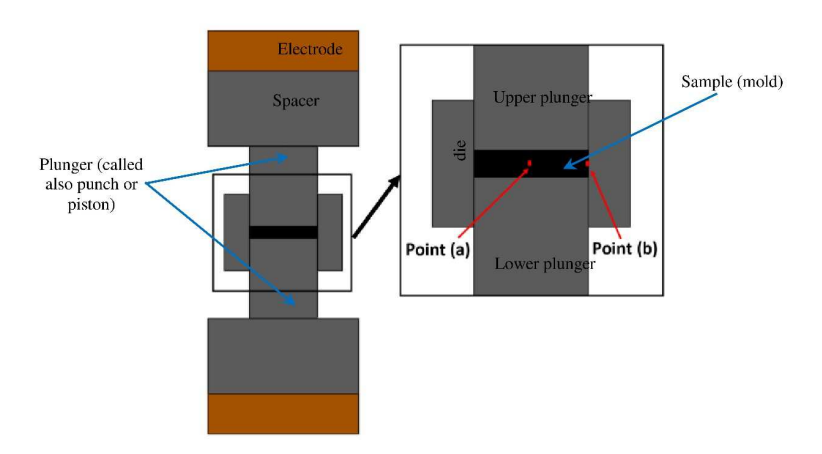


Fig. 3. Schematic representation of the location of Point (a) (placed in the middle of the sample) and Point (b) (placed at the edge of the sample). Note that the sintering graphite mold that gives the final shape of the sample (sintered material) is the area between the die and the punch (plunger) of the machine.



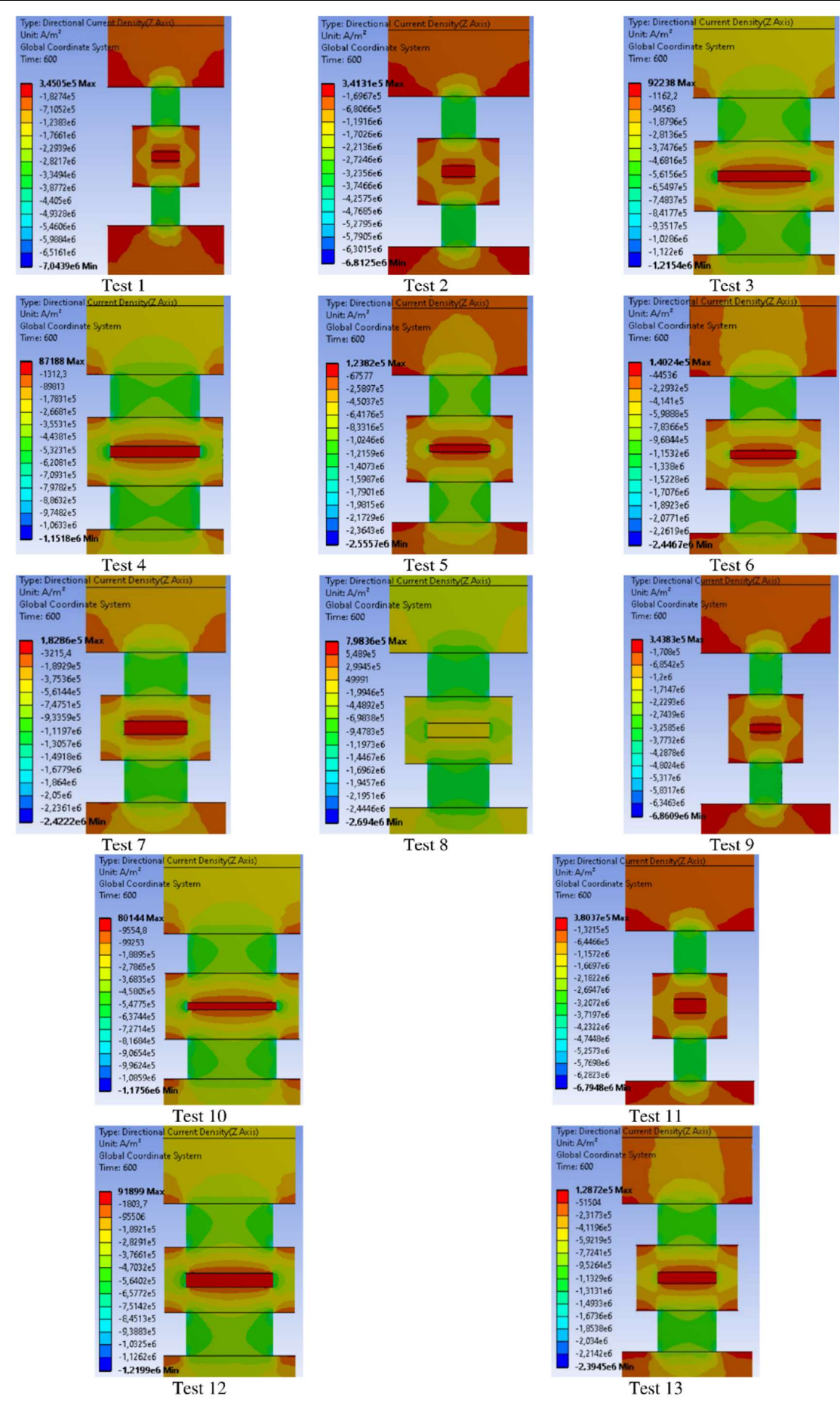


Fig. 4. Cross-sectional electric current density distributions in the SPS machine and in particular in the plunger/die/sample system region, calculated for all tested configurations at t = 600 s).



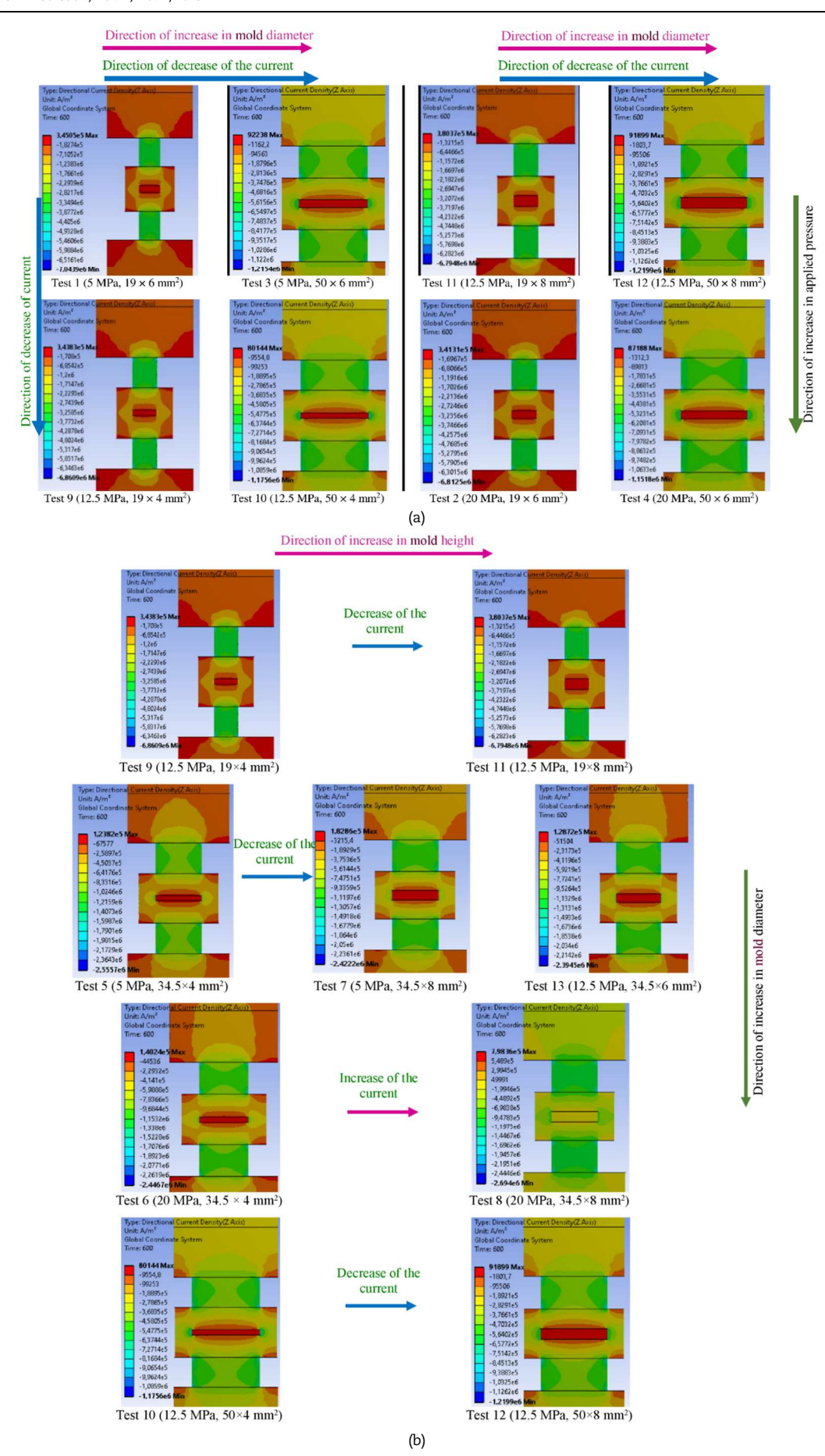


Fig. 5. (a) Pairs of tests with the same applied pressure and molds having the same height but having different diameters namely (19 and 50 mm), (b) Pairs of tests with the same pressure applied and molds having the same diameter but having different heights namely (4 and 8 mm), (c) Pairs of tests with same dimensions of the mold and with different applied pressures (5 and 20 MPa).



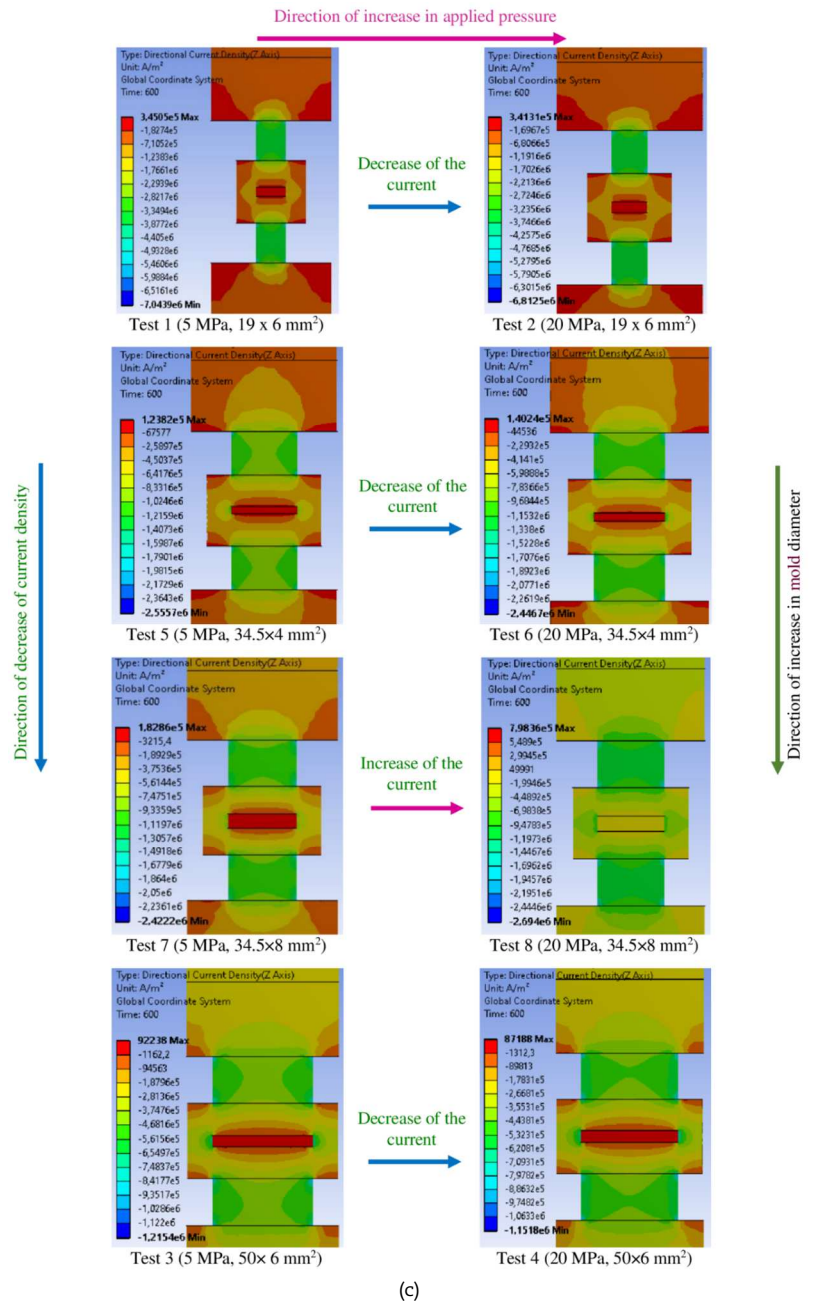


Fig. 5. Continued.

(i) Effect of increasing mold diameter on electric current distribution

Figure 5(a) groups the results of the electric current density distribution obtained from pairs of tests carried out with the same applied pressure and molds having the same height but different diameters, namely (D=19 and 50 mm). The pairs of tests are (1 and 3), (9 and 10), (11 and 12) and (2 and 4), respectively. Comparing the results of each of the two pairs of tests shows that increasing the diameter of the mold leads to a significant decrease in the intensity value of the electric current density in the plunger/die/sample system [9]. The examination also shows that the patterns of current density distributions in the system for the tests carried out with D=19 mm are almost similar and independent of the value of applied pressure. The same results can be observed by comparing the current density distribution patterns in the system for tests carried out with D=50 mm. Thus, the "applied" pressure and the mold height have little effect on the electric current patterns in the system and it is therefore expected that these parameters will only cause an insignificant decrease in the electric current values in the system. The effects of pressure and mold height are illustrated in the following two subsections.

(ii) Effect of increasing mold height on electric current distribution

Figure 5(b) groups the results of the electric current density distribution obtained from pairs of tests carried out with the same applied pressure and molds having the same diameter but different heights, namely (H = 4 and 8 mm). The test pairs are (9 and 11), (5 and 7), (6 and 8), and (10 and 12), respectively. Comparison of the results obtained for each pair of tests shows that generally the increase in the height of the mold leads to a decrease in the intensity value of the current density in the plunger/die/sample system, with the exception of the pair of tests (6 and 8) where an increase in the intensity and a change in the direction of the electric current are observed. Moreover, the distribution patterns of electric current density are almost similar for each pair of tests performed.



To show the effect of mold height on electric current, consider the test pair (9 and 11) as an example. Comparing the results, it can be seen that an increase in the mold height from 4 mm to 8 mm leads to a decrease in the maximum value of the electric current density in the SPS machine from the value $-6.86 \times 106 \text{ A/m}^2$ for test 9 to the value $-6.79 \times 106 \text{ A/m}^2$ for test 11, respectively. Note that the sign (-) indicates the direction of current movement; and the minus means that the direction is opposite to the direction of current movement. Obviously, this increase in the height of the mold increases the value of the current density in the sample from $3.43 \times 105 \text{ A/m}^2$ for test 9 to $3.8 \times 105 \text{ A/m}^2$ for test 11, respectively. It should be noted here that the currents in the nonconducting sample are obviously almost negligible compared to the average current reached in the SPS machine (with a ratio of about 1/18 which is negligible). On the other hand, comparing the pairs of tests (5, 7) and (6, 8) and test 13 between them since they were carried out with the same mold diameter, D = 34.5 mm, it can be observed that at the sample level, the highest current density is observed in the mold configurations that have the greatest height (i.e. tests 7 and 8) and that it decreases with the reduction of the mold height. It can be concluded that the increase in the mold height increases the value of the electric current density in the sample. The alumina sample therefore acts as an obstacle to the flow of electric current as shown by the results of reference [27]. Thus, increasing the mold height, which results in an increase in the volume of the sintered sample, leads to an increase in the current density inside the sample.

(iii) Effect of increasing the applied pressure on electric current distribution

Figure 5(c) groups the results of the electric current density distribution obtained from pairs of tests carried out with the same dimensions (diameter and height) of the mold and with different applied pressures, namely (5 and 20 MPa). The test pairs are: (1 and 2), (5 and 6), (7 and 8), and (3 and 4), respectively. Comparison of the results of each of the two pairs of tests shows that the increase in the applied pressure affects the distribution of the density of the electric current in the plunger/die/sample system, but less significantly compared to the effects of the size (dimensions D and H) of the mold discussed previously. This observation can be confirmed for example by the comparison between the pair of tests (1 and 2) where we see that the maximum current density value for test 1 is greater than that of test 2 (see Fig. 4c). This inverse relationship (disproportionate ratio) between the value of the applied pressure and the intensity of the electric current density is observed for most of the other pairs of tests which were carried out with the same mold size (namely (5 and 6), (3 and 4)). This is because increasing the applied pressure (which represents a compressive load) causes an increase in mechanical stress and strain, which in turn increases the cross-sectional area (throughout the system in our case) as the axial compression causes radial expansion, thus reducing the electric current density in the plunger/die/sample system. However, in the case of the pair of tests (7 and 8), it can be seen that despite the same size of the mold, it is observed that the increase in the applied pressure increases the maximum value of the current density; this is due to the high value of the height of the mold (which is H = 8 mm). This contradiction can be further clarified by comparing the percentage difference between the electric current density results from the pair of tests (1 and 2, performed with a mold height of H = 6 mm), and the results obtained from the pair of tests (5 and 6, carried out with H = 4 mm). The percentage differences are 3.28% and 4.26%, respectively. It can therefore be seen that increasing the mold height decreases the percentage difference in current density between tests (1 and 2), although the current density value is higher in tests (1 and 2) than in tests (5 and 6).

Finally, it can be concluded that increasing the applied pressure value only slightly affects the electric current density results; but it is the height and diameter of the mold that are the main parameters controlling the electric current density in the plunger/die/sample system and in the whole SPS machine.

- Thermal behavior

The graphs in Figs. 6(a) to 6(c) show the time evolutions of the temperature at point (a) (located in the middle of the sample as shown in Fig. 3) predicted for all tests during the sintering period. Unlike the previous cases and as is obvious, we have divided/grouped and represented together the results of the tests that reached very close temperatures in order to be able to compare the tests between them. Indeed, we have grouped (i) in Fig. 6(a) the tests where the maximum temperature reached is of the order of [1000 - 1100 K] and having a mold diameter D = 19 mm, namely tests 1, 2, 9 and 11, (ii) in Fig. 6(b) the tests where the maximum temperature reached is of the order of [500 - 600 K] and having a mold diameter D = 34.5 mm, namely tests 5, 6, 7, 8 and 13, and (iii) in Fig. 6(c) the tests where the maximum temperature reached is of the order of [400 - 500 K] and having a mold diameter D = 50 mm, namely tests 3, 4, 10 and 12.

Examination of the curves in Figs. 6(a) to 6(c) shows that increasing the mold diameter significantly reduces the maximum temperature reached in the sample for each class of tests [9]. Indeed, if we consider for example Fig. 6(a) which shows as indicated above the temporal evolutions of the temperature at point (a) of the sample predicted for tests 1, 2, 9 and 11 (i.e. all the tests carried out with a mold diameter D = 19 mm) during the sintering time. It can be noted that the highest temperature is observed in the configuration of test 11 and the lowest temperature is observed in that of test 9; while tests 11 and 11 present intermediate temperature values. These temperature differences are exclusively due to the increase in the height of the mold since the applied mechanical pressure has no significant effect on the temperature [5, 28, 29], which results in an increase in the temperature value reached in the sample.

Furthermore, comparing the curves in Fig. 6(b) (all tests performed with D = 34.5 mm) with each other and the curves in Fig. 6(c) (all tests performed with D = 50 mm) with each other, we see the same trends as those shown by the curves in Fig. 6(a). We can therefore conclude that the maximum temperature value always occurs in the configurations with the greatest mold height. Furthermore, it should be noted on the one hand that for all the mold sizes tested, the maximum temperature in the sample is obtained in test 11, with a maximum value of 1105.3 K; this is the test that corresponds to the mold size with the greatest height (H = 8 mm) and the smallest diameter (D = 19 mm). Note that this test 11 also recorded the highest current density in the sample. On the other hand, the lowest temperature of all the tests is obtained in test 10, with a maximum value of 468.03 K; this test 10 which corresponds to the mold size (having the smallest height (H = 4 mm) and the largest diameter (D = 50 mm)) also recorded the lowest current density in the sample. It can therefore be concluded that the increase in the height of the mold and the decrease in its diameter lead to an increase in the temperature reached in the sample.

3.2. Mechanical behavior

- Von-Mises stress analysis

Figure 7 shows the three-dimensional and cross-sectional views of the Von-Mises stress distributions in the sample, calculated for all tested configurations at the end of the sintering process (at time $t=600\,\mathrm{s}$). Inspection of this figure shows that depending on the applied pressure and the dimensions (diameter and height) of the mold, several mechanical trends can be identified and in particular Fig. 6 can be divided into the following three groups of Figs. 8(a)-(c).



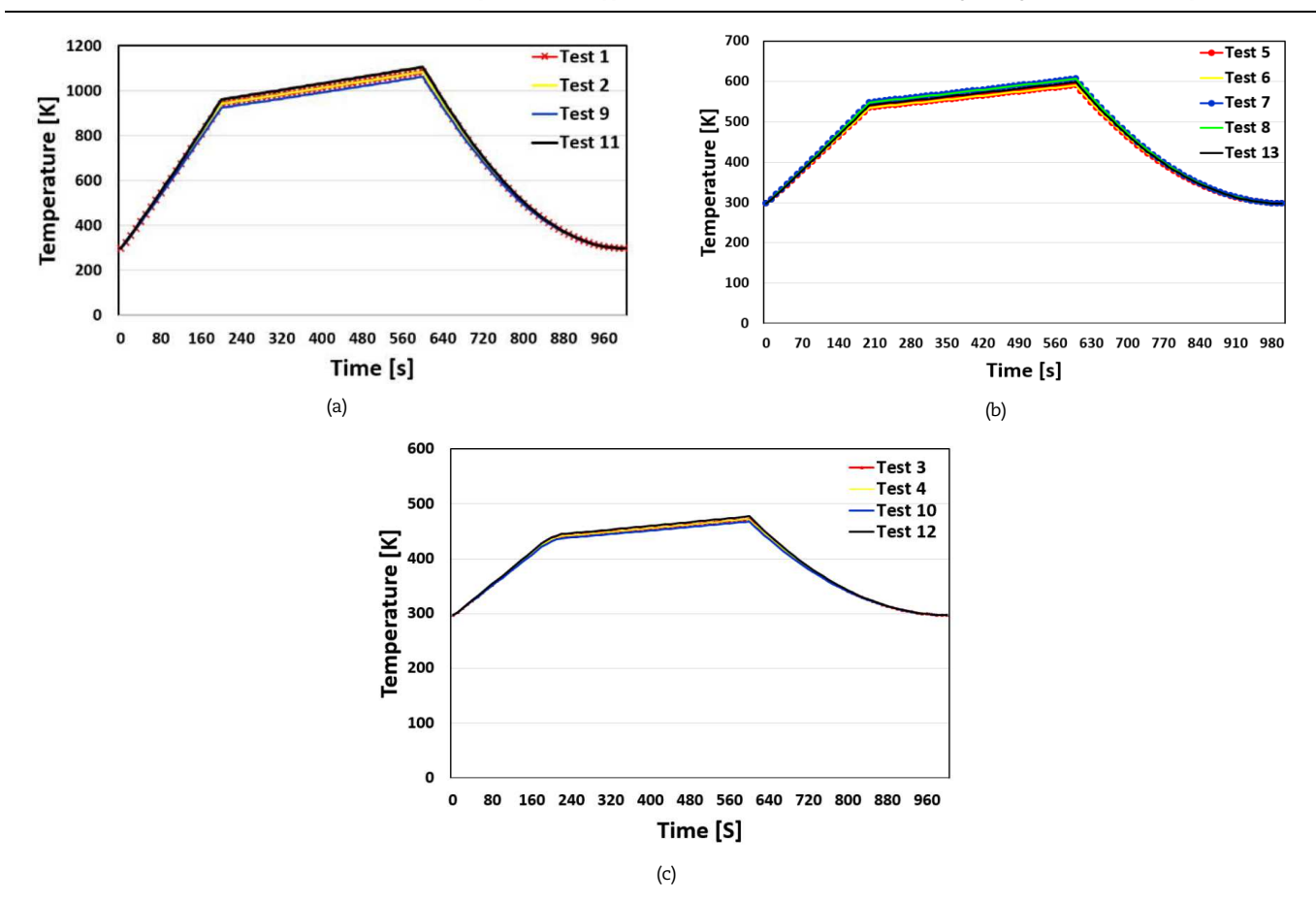


Fig. 6. (a) Temperature variations over time at point (a) of the sample for tests 1, 2, 9 and 11 (Class of tests performed with diameter D = 19 mm), (b) Temperature variations over time at point (a) of the sample for tests 5, 6, 7, 8 and 13 (Class of tests performed with D = 34.5 mm), (c) Temperature variations over time at point (a) of the sample for tests 3, 4, 10 and 12 (Class of tests performed with D = 50 mm).

(i) Effect of increasing the applied pressure on the stress distribution

Figure 8(a) groups pairs of tests carried out with the same dimensions (diameter and height) of the mold and with different applied pressures, namely 5 and 20 MPa. The test pairs are: (1 and 2), (5 and 6), (7 and 8), and (3 and 4), respectively. Comparison of the results of each pair of tests shows that the increase in the applied pressure leads to an increase in the value of the Von-Mises stress in the sample. This finding has been demonstrated in works [2-5].

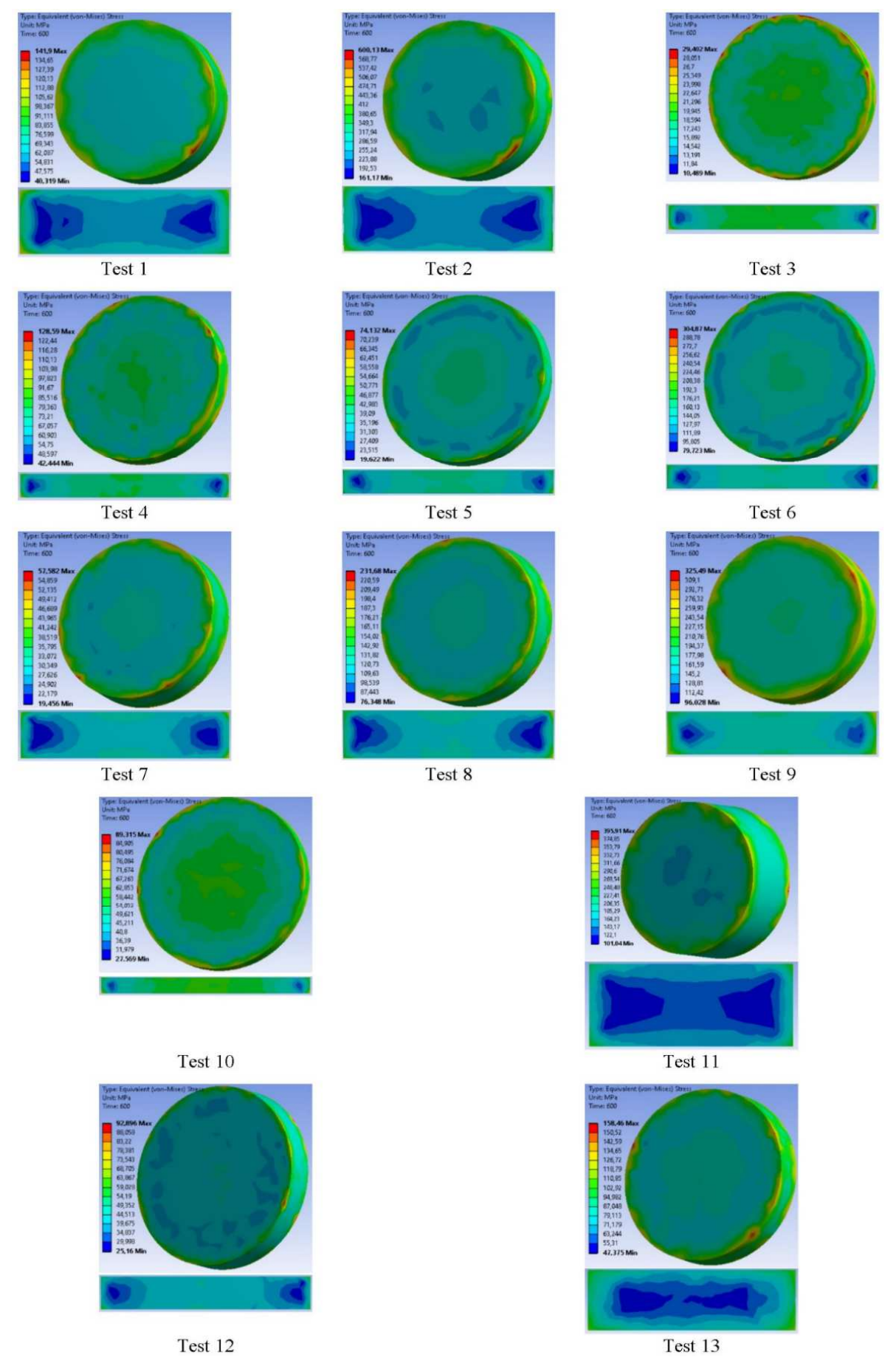
(ii) Effect of increasing mold diameter on stress distribution

Figure 8(b) groups pairs of tests carried out with the same applied pressure and molds having the same height but having different diameters, namely 19 and 50 mm. The test pairs are (1 and 3), (9 and 10), (11 and 12), and (2 and 4), respectively. Similar trends (as above (case "(i)")) are also observed when comparing each of the pairs of tests. In fact, the trends shown by Figs. 8(a) and 8(b) due to the effects of increasing applied pressure and mold diameter are expected and justified by the laws of mechanics (namely Hooke's Law).

(iii) Effect of increasing mold height on stress distribution:

Figure 8(c) groups pairs of tests carried out with the same applied pressure and molds having the same diameter but having different heights, namely 4 and 8 mm. The test pairs are (5 and 7), (6 and 8), (10 and 12) and (9 and 11), respectively. Contrary to the trends shown by cases "(i)" and "(ii)" above, it is observed here that the increase in the mold height affects the mechanical behavior of the sample and consequently the value and distribution of the Von-Mises stress in the sample. Indeed, the increase in height of the mold leads to a decrease in the value of the stress in the sample for the test pairs (5 and 7) and (6 and 8) and an increase in the value of the stress for the pairs of tests (10 and 12) and (9 and 11). Furthermore, it should be noted that the observed decrease in the value of the Von-Mises stress is significant in the test pairs (5 and 7) and (6 and 8); while the observed increase in the value of this stress is significant for the test pair (9 and 11) but it is insignificant for the test pair (10 and 12). The difference between these three classes of mechanical behavior lies in the value of the mold diameter; therefore, it can be said that the effect of increasing the mold diameter affects the increase in the mold height. Therefore, the effect of increasing the mold height is related to the effect of increasing the mold diameter. This observation leads us to examine the effect of thermal stresses, which are responsible for these results. Take for example the pair of tests (9 and 11) where the mold diameter is 19 mm, the temperature difference observed between tests 9 and 11 is of the order of 45 K. This difference has a considerable impact (effect), especially considering the maximum temperature value reached in the sample (greater than 1100 K); this generates numerous thermal stresses in the mold which has the greater height i.e. test 11. Consequently, the stress value is higher in test 11 than in test 9. However, the maximum temperatures reached in the sample for the test pairs (5 and 7) and (6 and 8) are almost identical for the two test pairs and are of the order of 600 K. Also, the differences temperature in the sample between the two tests of each pair are almost identical and of the order of 16 K. The relatively low temperature reached, compared to that reached for test 11, does not cause any significant thermal stress. Thus, the decrease in stress due to the increase in height of the mold cannot be compensated by thermal stresses at this temperature difference and at this low temperature (600 K), thus explaining why the stress value in test 5 is higher than in test 7; the same is true for tests 6 and 8.





 $\textbf{Fig. 7.} \ \textbf{Three-dimensional and cross-sectional views of the Von-Mises stress distribution in the sample at time $t=600$ s for all tests.}$



On the other hand, it should be noted that although the temperature reached in the sample during the couple of tests (10 and 12) is low (of the order of 470 K) and the temperature difference between each test is small (of the order of 10 K), the results show that the maximum Von-Mises stress reached in test 12 (where H = 8 mm) is slightly higher than that reached in test 10 (where H = 4 mm). Moreover, the minimum stress value reached in test 12 is lower than that reached in test 10. Thus, it can be concluded that although the stresses seem lower in test 12, they are concentrated in the critical areas (the ends of the sample (see distribution of Von-Mises stresses for test 12 in Fig. 8(b))); this concentration still leads to an increase in the maximum stress value despite the increase in the height of the mold. Finally, it can be concluded that it is crucial to carefully choose the sintering parameter (applied pressure) as well as the size (diameter and height) of the mold to obtain a more homogeneous stress distribution leading to more homogeneous properties of the samples produced by the SPS process.

Axial stress study

Figures 9(a)–(c) show the predicted axial stress values, σz, along the sample diameter from "point (a)" to "point (b)" up to the die tip (see Fig. 3), for "all tests performed" at time t = 600 s. Inspection of these figures shows that the maximum axial stress value is at point (b) (i.e. the tip of the sample) for all tests. As with the thermal study above, we have divided/grouped and plotted the results: (i) in Fig. 9(a) the tests with a mold diameter of 19 mm (i.e. tests 1, 2, 9 and 11), (ii) in Fig. 9(b) the tests with a mold diameter of 34.5 mm (i.e. tests 5, 6, 7, 8 and 13), and (iii) in Fig. 9(c) the tests with a mold diameter D = 50 mm (i.e. tests 3, 4, 10 and 12). Comparing the curves of tests (9 and 11 of Fig. 9(a)), ((5 and 7) and (6 and 8) of Fig. 9(b)) and (10 and 12 of Fig. 9(c)), it is observed that the increase in the mold height decreases the maximum value of the axial stress (at point (b)) for all these tests. However, the axial stress at point (a) exhibits a different behavior. Indeed, in tests (9 and 11) and (10 and 12), the increase in the mold height decreases the value of the axial stress at point (a); whereas in tests (5 and 7) and (6 and 8), the increase in the mold height increases the value of the axial stress at point (a). This behavior justifies our explanations in the previous discussion of the Von-Mises stress results. On the other hand, comparing the difference between the maximum and minimum values of axial stress in the sample, calculated for all tests in Figs. 9(a), 9(b) and 9(c), it can be observed that the smallest difference appears in test 3, where it is observed that the axial stress values obtained for this test are low because the lowest pressure (5 MPa) was applied and the mold diameter was the largest (50 mm). While the largest difference appears in test 2, where it is observed that the axial stress values are the highest because the highest pressure (20 MPa) was applied and the mold diameter was the smallest (19 mm). Therefore, it can be concluded that the applied mechanical pressure increases the difference between the maximum and minimum values of axial stress.

Furthermore, comparing the curves of all tests (in Fig. 9(a), 9(b) and 9(c)), it is observed that increasing the mold height decreases the difference between the maximum and minimum values of axial stress in the sample (this observation is valid for all curves), which makes the axial stress values converge (makes them smoother) and therefore ensures greater homogeneity in the axial stress distribution in the sample. Thus, increasing the mold height allows to obtain a more homogeneous stress state in the sample.

Finally, by analyzing the curves of tests 5, 6, 9 and 10, it is observed that a very significant decrease in the value of the axial stress at the points close to the end of the sample has taken place; this decrease is followed by a significant increase in the value of the axial stress up to point (b). The relationship between these tests is that the height of the mold (H) is equal to 4 mm. This confirms the previous observation that the increase in the height of the mold ensures a certain degree of homogeneity in the distribution of axial stresses in the sample and therefore allows to have an increased homogeneity in the properties of the alumina material produced by the SPS process.

3.3. Analysis of the results and optimization of the SPS parameter applied pressure and mold size

The Box-Behnken Design of Experiments (BBD) is an effective statistical method for optimizing experimental processes by exploring the interactions between several factors. This design is based on a set of experimental points located at the center of the faces of the experimental domain, which allows for an accurate estimation of quadratic effects without requiring experiments at the vertices of the cube. This approach reduces the total number of experiments while ensuring reliable modeling of the responses.

The analysis of the results obtained by the BBD is generally performed using an analysis of variance (ANOVA), which evaluates the statistical significance of the main effects and interactions between factors. This analysis compares the variability explained by the model to that attributable to experimental errors. A significance test is then applied to identify influential terms, thus facilitating the selection of a robust predictive model. In addition, the analysis includes an assessment of the adequacy of the model, verifying the consistency between the experimental and predicted values. Thus, the combination of the Box-Behnken experimental design and the analysis of variance makes it possible to optimize a process while minimizing errors and guaranteeing a solid interpretation of the experimental results [14-20]. Recall here some equations that explain how both the Box-Behnken method and ANOVA work:

- Box-Behnken Design of Experiments (BBD)

The Quadratic Polynomial Model (Response Surface Model) is expressed as:

$$y = \beta_0 + \sum_{i=1}^k \beta_i x_i + \sum_{i=1}^k \beta_{ii} x_i^2 + \sum_{i=1}^k \sum_{i < j}^k \beta_{ij} x_i x_j + \delta$$
 (1)

where y is the predicted response, x_i and x_j are the factors, k is the number of factors and δ is the random error term. In addition, the regression coefficients including β_0 which is a constant term (the intercept), β_i are the coefficients for the linear effects of each factor, β_{ii} are the coefficients for the quadratic effects (to capture curvature), β_{ij} are the coefficients for the interaction effects between factors. Additionally, the regression coefficients include: β_0 , which represents a constant term (the intercept); the β_i coefficients, representing the linear effects of each factor; the β_{ii} coefficients, which capture the quadratic effects to model the curvature; and the β_{ij} coefficients, representing the interaction effects between factors. This equation models the relationship between the factors and the response by including both linear, quadratic, and interaction effects, which is essential for optimization in BBD.

- ANOVA Method

The partitioning of the Total Sum of Squares in ANOVA is expressed as:

$$SST = SSR + SSE \tag{2}$$

where SST (total sum of squares) is the total variability of observations relative to the overall mean, SSR (sum of squares for regression) is the variability explained by the model (i.e., variation due to factors), and SSE (sum of squares for error) is the unexplained variability (i.e., residual or error variation).





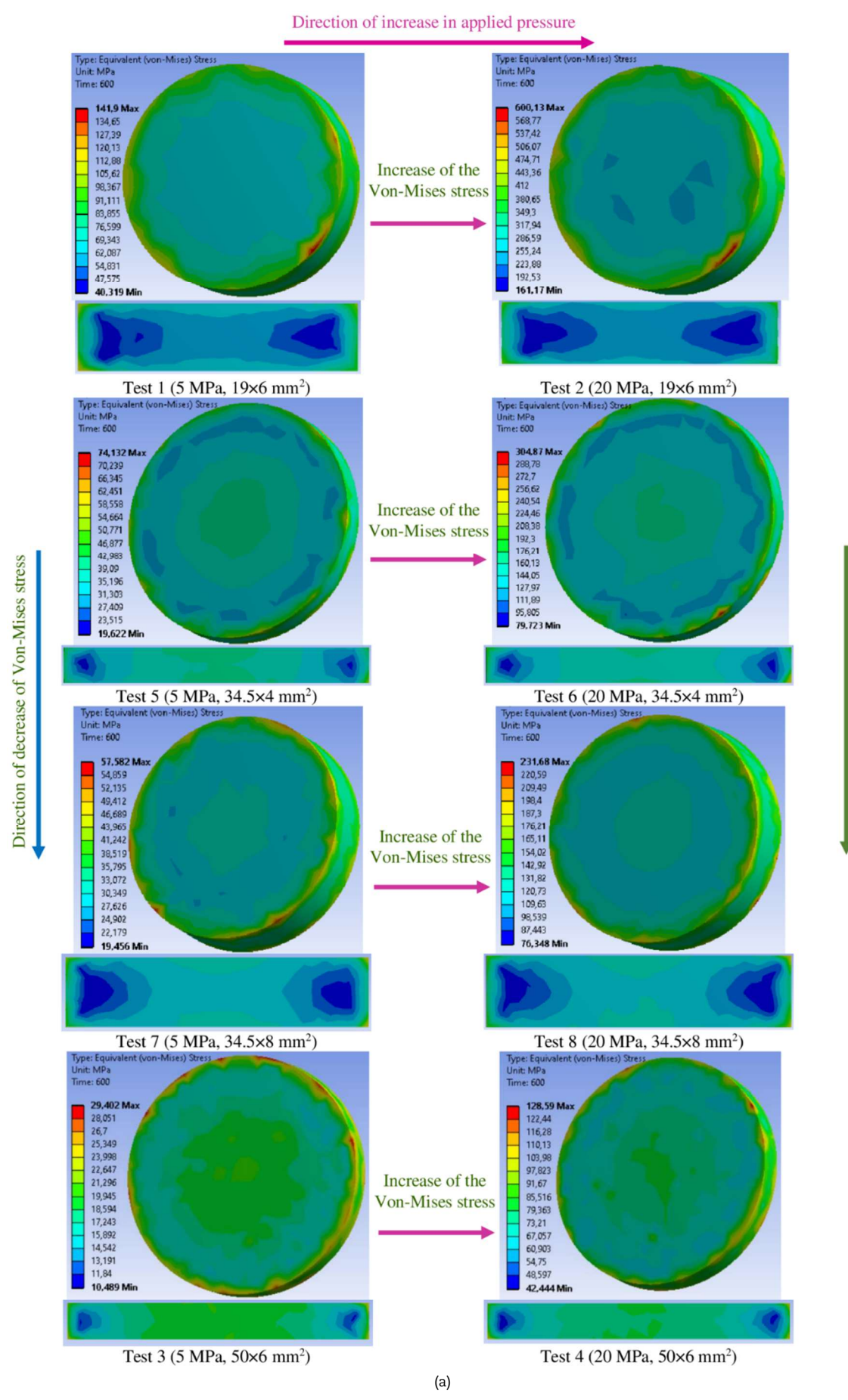
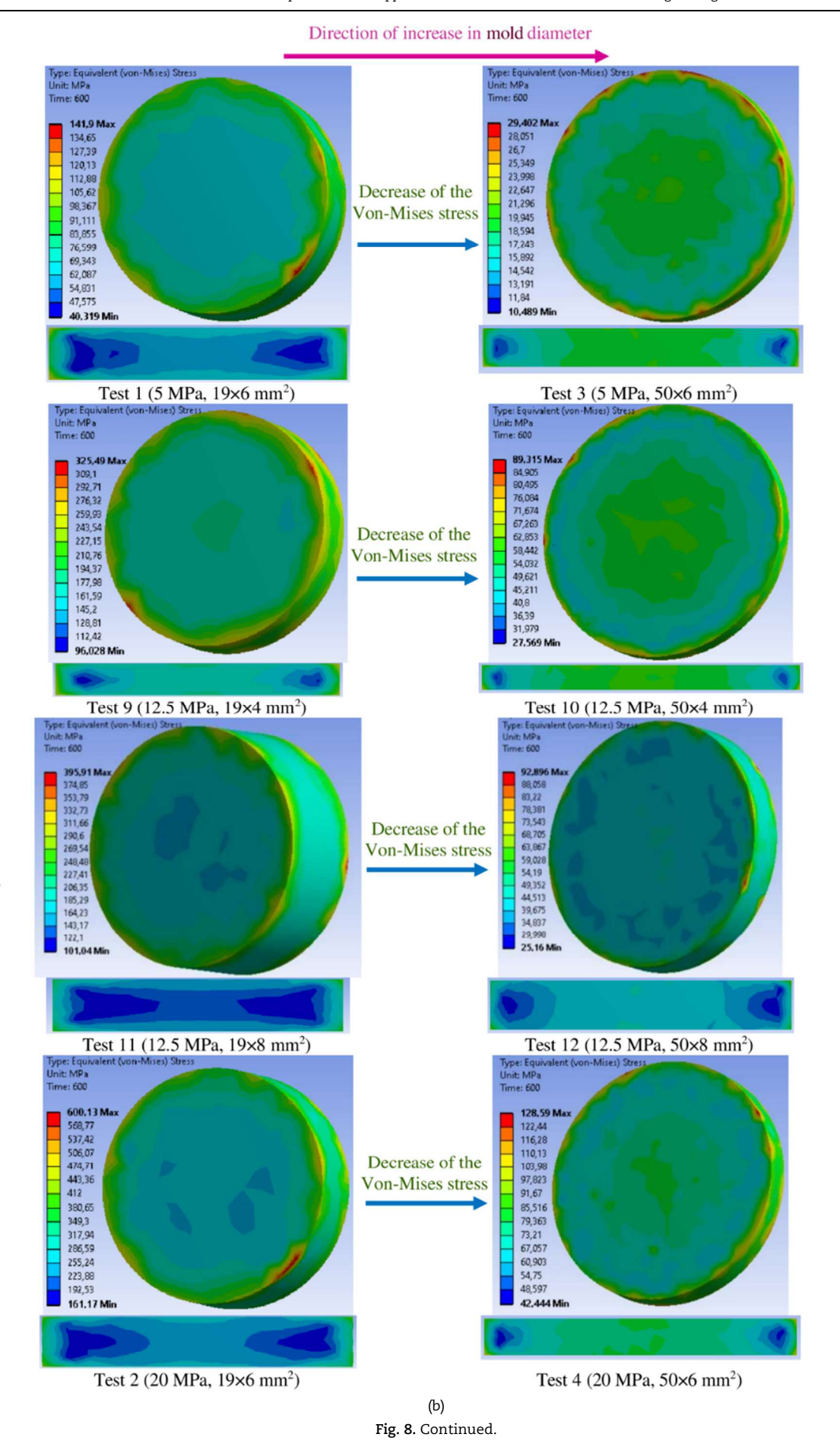
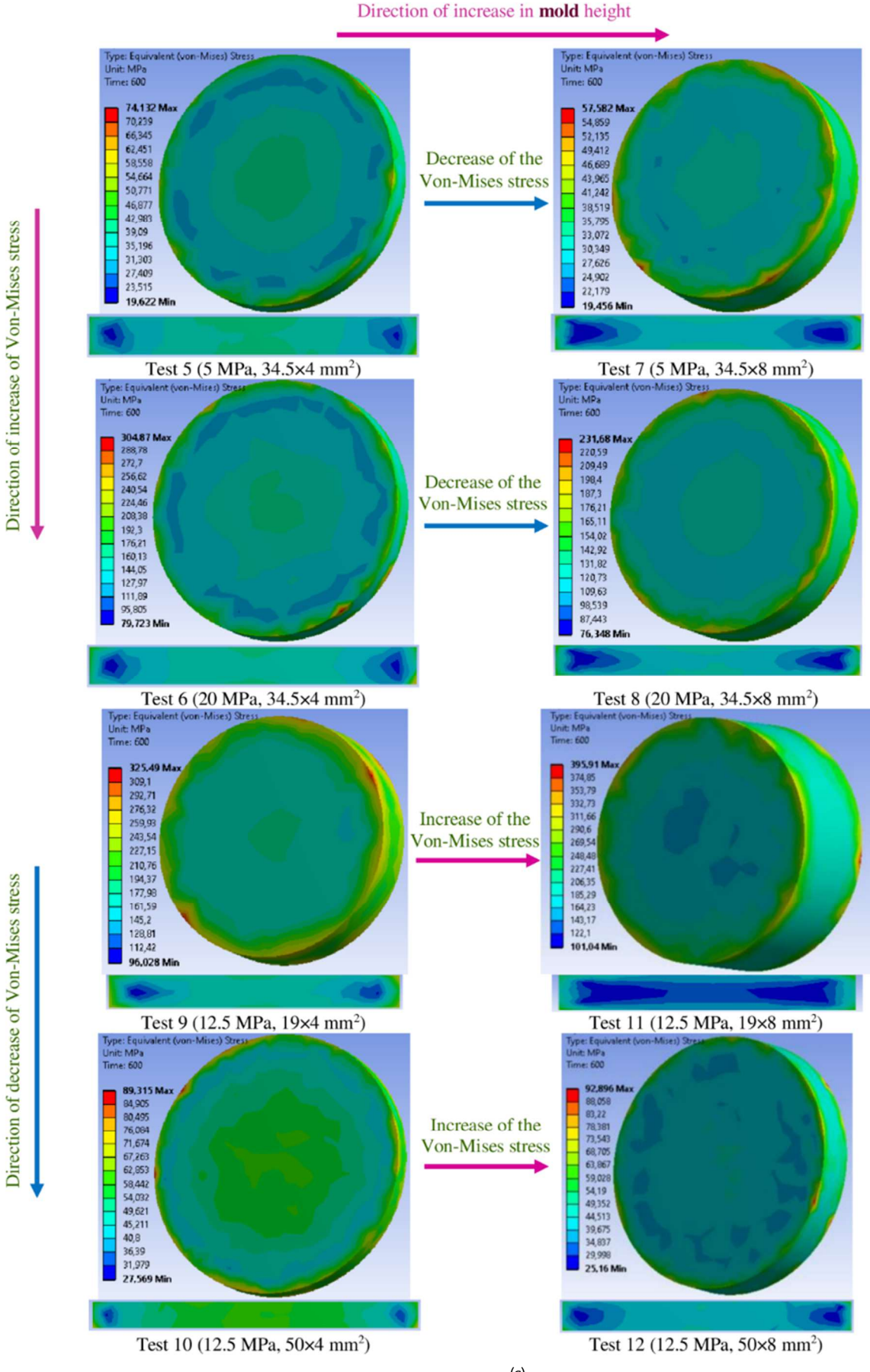


Fig. 8. (a) Pairs of tests with same dimensions of the mold and with different applied pressures (5 and 20 MPa), (b) Pairs of tests with the same applied pressure and molds having the same height but having different diameters namely (19 and 50 mm), (c) Pairs of tests with the same pressure applied and molds having the same diameter but having different heights namely (4 and 8 mm).



Direction of increase of Von-Mises stress



(c) Fig. 8. Continued.



This relation decomposes the total observed variability into the part explained by the model and the part due to error, thereby helping to assess the model's performance.

- F-statistic in ANOVA

The F-Statistic is used for testing the significance of the model and it is expressed as:

$$F = \frac{MSR}{MSE} = \frac{SSR/df_R}{SSE/df_E}$$
 (3)

Here, the Mean Square Regression (MSR) is calculated as SSR divided by the degrees of freedom for regression (df_R) , and the Mean Square Error (MSE) is calculated as SSE divided by the degrees of freedom for error (df_E) .

In the ANOVA method, the F statistic is used to test the null hypothesis that the model does not explain a significant portion of the variability in the response. A high F value indicates that the model is statistically significant.

- Application to the optimization of SPS parameters

The above optimization procedure, which consists of applying the Box-Behnken Plan of Experiments (BBD) and the ANOVA Method, allows to determine the sintering parameters of a material from simple SPS experiments. Its main advantage lies in the rapidity with which it allows to obtain these parameters, requiring only a few SPS tests, unlike traditional approaches that require a large number of mechanical tests and long periods of experimentation and characterization. The modeling of the uniaxial compaction of a complex shape reveals an excellent agreement between experimental results and simulations, highlighting the problem of differences in shrinkage height, which generate areas with high porosity gradients [1-3]. Many studies have emphasized the importance of controlling the sintering parameters to produce a more homogeneous material and obtain a uniform microstructure. On the other hand, some experiments have failed due to an inappropriate choice of the sintering parameters of the samples [5-9].

- Analysis of results

Figures 10(a)–(c) show the surface diagrams illustrating respectively (a) the effect of applied pressure and selected mold height, (b) the effect of applied pressure and selected mold diameter, and (c) the effect of selected mold height and diameter on the value of the percentage difference of Von-Mises stresses in the sample. These plots were developed based on the value of the percentage difference of Von-Mises stresses in the sample at t = 600 s. In fact, this percentage difference is equal to the difference between the maximum value of Von-Mises stress and the minimum value of Von-Mises stress divided by the maximum value of Von-Mises stress. The calculated difference must be multiplied by 100 to obtain the percentage value, i.e. Percentage difference = % difference = $|((\sigma_{e_{max}} - \sigma_{e_{min}})/\sigma_{e_{max}})| \times 100$. The analysis of the percentage difference values was chosen in order to determine the optimal values that would guide us towards obtaining the smallest percentage difference value. Thus, our goal is to minimize the maximum values and maximize the minimum values of the Von-Mises stress, in order to reduce the difference of stress values in the sample and thus converge/smooth and obtain a more homogeneous stress distribution, thus ensuring more homogeneous material properties, and ensuring the production of samples of optimal homogeneity by SPS.

(a) Effect of applied pressure and selected mold height on the percentage difference in Von-Mises stress

Examination of Fig. 10(a) shows that increasing the mold height decreases the value of the percentage difference in Von-Mises stress for the lowest and highest-pressure values; however, it increases the value of the percentage difference for the average pressure values. Furthermore, the lowest percentage difference values were found when applying the lowest and highest-pressure values using the largest mold height value; these parameters therefore represent the best sintering parameters to select. On the other hand, the highest percentage difference values were found when applying the highest and lowest pressure values using the lowest mold height; these parameters therefore represent the worst sintering parameters to select.

(b) Effect of applied pressure and selected mold diameter on the percentage difference in Von-Mises stress

Examination of Fig. 10(b) shows that increasing the applied pressure value, using the smallest value of the mold diameter, increases the percentage difference of the Von-Mises stresses in the sample. Whereas using the average value of the mold diameter, it is observed that increasing the pressure has only a small effect (impact) on the value obtained for the percentage difference. Finally, using the largest value of the mold diameter, it is observed that increasing the pressure value up to the average value increases the value of the percentage difference of the Von-Mises stress in the sample; whereas further increasing the pressure above its average value decreases the value of the percentage difference.

(c) Effect of selected mold height and diameter on the percentage difference in Von-Mises stress

Examination of Fig. 10(c) shows that increasing the mold height using its "smallest" diameter increases the percentage difference of Von-Mises stress in the sample. Furthermore, increasing the mold height using a medium (average) value diameter decreases the value of the percentage difference of Von-Mises stress in the sample. However, using a larger value of the mold diameter, it is found that increasing the value of the mold height beyond its "average" value decreases the value of the percentage difference in the Von-Mises stress in the sample. Further increasing the mold height to its maximum value increases the value of the percentage difference in the Von-Mises stress in the sample.

- Selection of optimal parameters using surface diagrams

Let us now move on to the analysis of the results presented in each surface diagram of cases (a) to (c) of Figs. 10. In fact, the analysis of each diagram allows to select the optimal conditions allowing the obtaining of more homogeneous alumina material as follows:

From the diagram of Fig. 10(a)

- The maximum Von-Mises stress difference percentage value is reached when using: (H = 4 mm; P = 5 MPa) and (H = 4 mm; P = 20 MPa).
- The optimum Von-Mises stress difference percentage value is reached when applying: (H = 8 mm and P = 5 MPa) and (H = 8 mm and P = 20 MPa).

From the diagram of Fig. 10(b)

- The maximum Von-Mises stress difference percentage value is reached when using: (D = 19 mm and P = 20 MPa).
- The optimum Von-Mises stress difference percentage value is reached when using: (D = 50 mm and P = 5 MPa) and (D = 50 mm and P = 20 MPa).



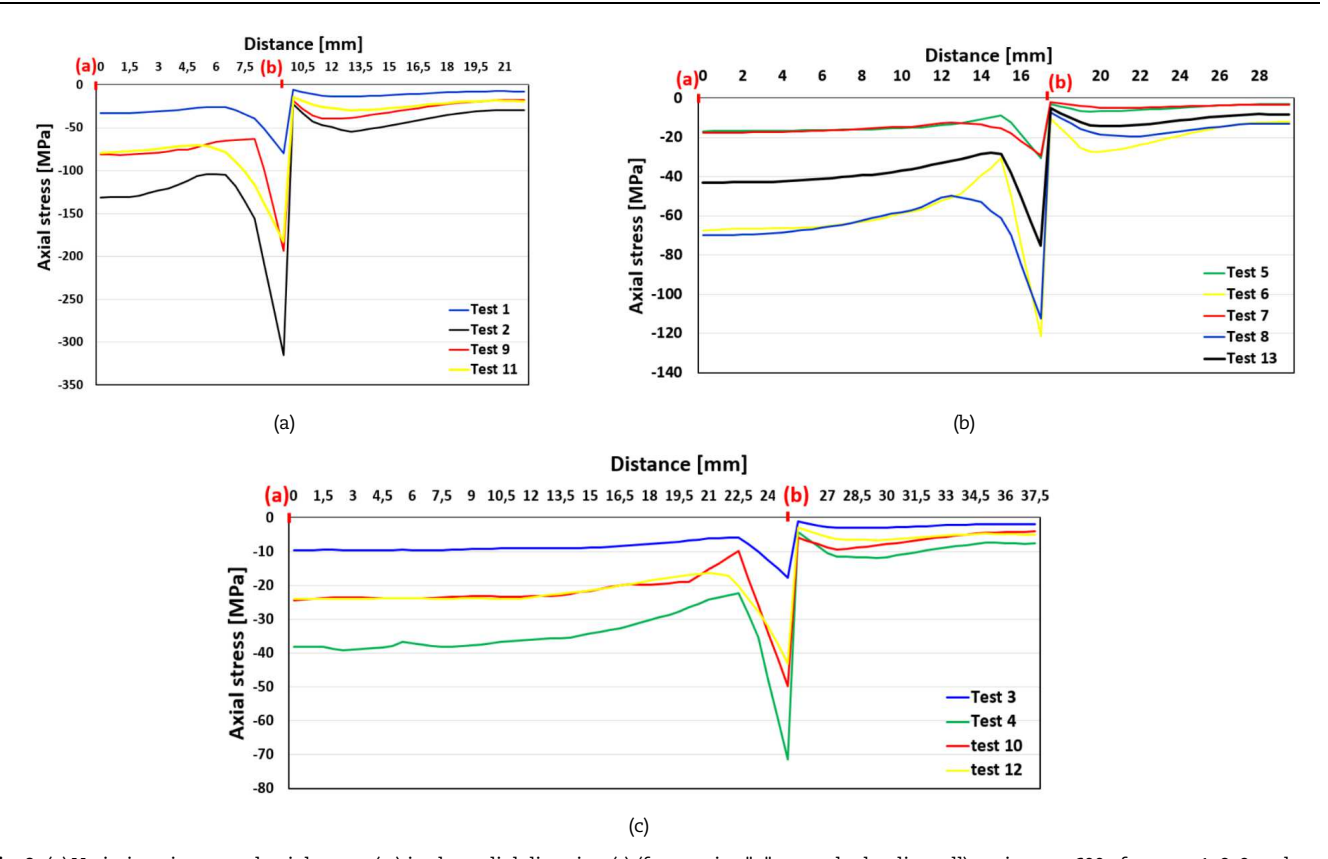


Fig. 9. (a) Variations in normal axial stress (σ_z) in the radial direction (r) (from point "a" towards the die wall) at time t = 600s for tests 1, 2, 9 and 11, (b) Variations in normal axial stress (σ_z) in the radial direction (r) (from point "a" towards the die wall) at time t = 600 s for tests 5, 6, 7, 8 and 13, (c) Variations in normal axial stress (σ_z) in the radial direction (r) (from point "a" towards the die wall) at time t = 600 s for tests 3, 4, 10 and 12.

• From the diagram of Fig. 10(c)

- The maximum Von-Mises stress difference percentage value is reached when using: (D = 19 mm and H = 8 mm) and (D = 50 mm and H = 8 mm).
- The optimum Von-Mises stress difference percentage value is reached when using: (D = 34.5 mm) and H = 8 mm.

From the results and analyses of the previous diagrams, we can finally conclude with the estimation of the optimal values of the SPS parameters (valid for our case study) such as (P = 5 MPa) or 20 MPa), (H = 8 mm) and (D = 34.5 mm) or 50 mm).

- Optimization of the SPS parameter "applied pressure" and mold size using the ANOVA method

After having developed the test plan and discussed and analyzed the results obtained by the surface diagrams, we can now move on to the optimization of the studied (tested) SPS sintering parameters related to our case study (applied pressure, and size (height and diameter) of the mold) allowing to obtain a homogeneous alumina material with the desired properties. To achieve this goal, we will set two optimization conditions to converge the maximum value to the minimum value of Von-Mises stress in the sample. Accordingly, we will seek the optimal values of the studied parameters to maximize the minimum value of Von-Mises stress and minimize the maximum value of Von-Mises (see Table 2). Moreover, the values found for the studied parameters (applied pressure and mold size) for our conditions must be validated by another additional test.

After running the optimization calculations using the ANOVA method, the optimal values of the studied parameters were found to obtain a material with the most homogeneous stress distribution and multiple response predictions, as shown in Table 3. These parameter values have already been applied to test 8 of our numerical calculation, so it will not be necessary to perform an additional validation test. Moreover, the results found by the ANOVA method align well with the values estimated in the previous surface plot analysis of the Von-Mises stress difference percentage.

Finally, Table 4 summarizes the results obtained by the ANOVA method for all the tests carried out in this work. These results allow to compare the effects of all the SPS parameters on the thermoelectric and mechanical behavior of the sample. It is clearly seen that the parameter values found for test 8 are the best to choose in order to obtain a homogeneous alumina material with the desired properties.

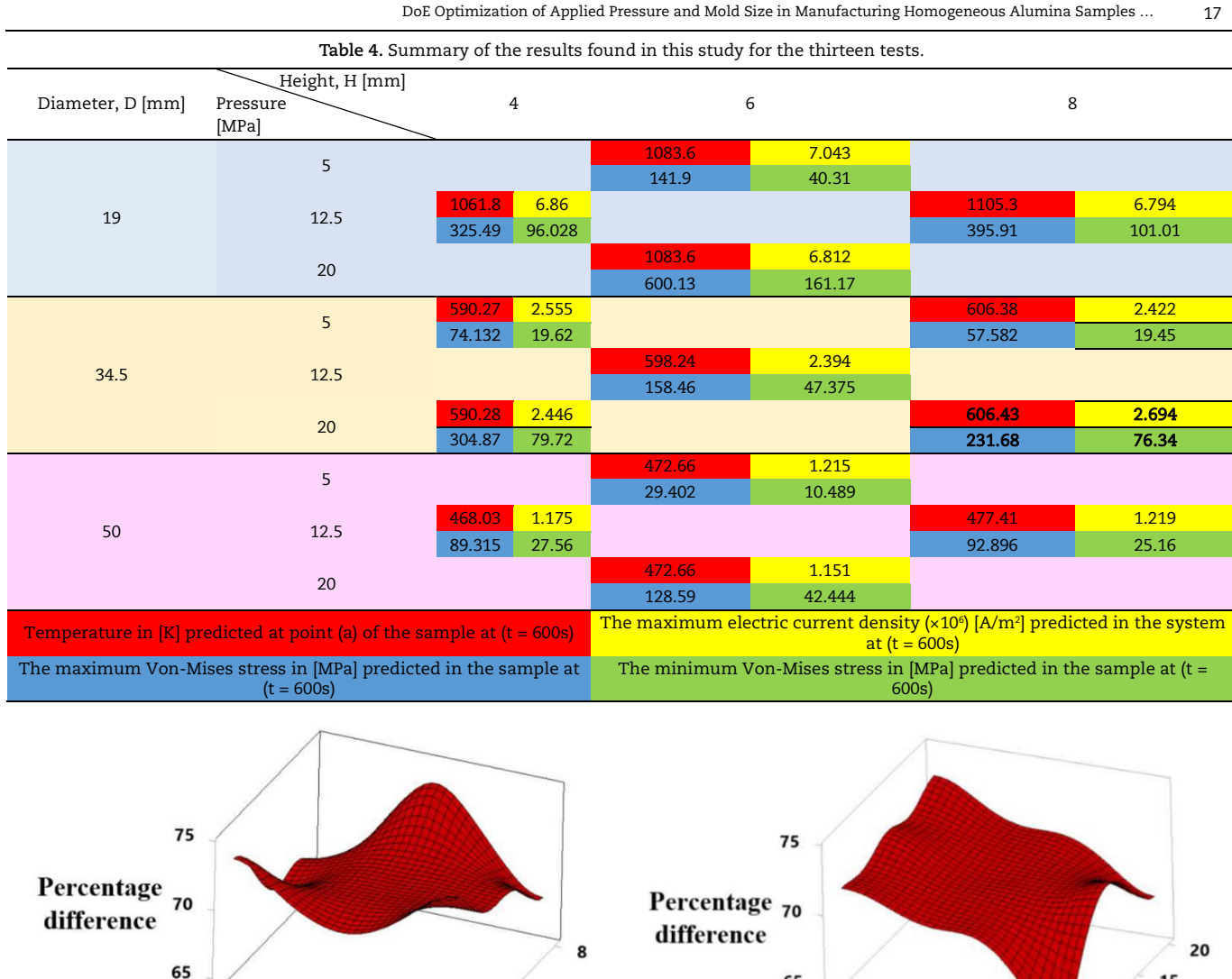
Table 2. Optimized plan found by the Box-Behnken method.

Response	Objective	Lower	Target	Higher
Stress MIN (MPa)	Maximum	10.489	161.170	_
Stress MAX (MPa)	Minimum		29.402	600.13

Table 3. ANOVA solution.

Variable	Configuration	
P (MPa)	20	
D (mm)	34.5	
H (mm)	8	





65 65 Н 10 5 20 15 40 D 50 (a) (b) Percentage difference 20 D (c)

Fig. 10. Surface plots showing the effect of the various parameters on the value of the percentage difference in Von-Mises stresses at the sample at time t = 600 s.

4. Conclusion

In this study, a Box-Behnken experimental design was designed to be used to perform the numerical calculation of the thermoelectric and mechanical behavior during SPS sintering of an alumina sample. The objective was to determine the optimal values of the tested parameters (applied pressure and mold size (dimensions)) for the fabrication of alumina samples with homogeneous properties by the SPS technique. The main conclusions from this study are as follows:



- Increasing the mold diameter leads to a significant decrease in the value of the electric current density.
- Increasing the mold height leads to a significant increase in the value of the electric current density.
- Increasing the applied pressure slightly affects the electric current density results.
- Increasing the mold height ensures a more uniform axial stress distribution, contributing to the homogeneity of the final material's properties
- Careful selection of the parameters, particularly the applied pressure, mold diameter, and height, is crucial to achieving a more homogeneous stress distribution, thereby ensuring uniform properties in the final sintered material.
- The optimum values of the parameters of SPS sintering of alumina applying an electric current of 1000 A are: an applied pressure of P = 20 MPa and a mold size having a height H = 8 mm and a diameter D = 34.5 mm.

These results highlight the importance of precise control of sintering parameters to optimize the quality and performance of alumina-based materials produced by SPS. Future work could explore the effects of varying other parameters, such as sintering time and temperature, to further refine the process and extend its applicability to other advanced ceramic materials.

Author Contributions

A. Kriba and F. Mechighel conceptualized the study and developed the methodology; F. Mechighel administered the project and managed its execution; A. Kriba and F. Mechighel designed the framework; A. Kriba developed the software programming; R. Djebali performed the optimization; A. Kriba prepared the original draft; A. Kriba, F. Mechighel, R. Djebali, and A.J. Chamkha reviewed and edited the manuscript; F. Mechighel, R. Djebali, and A.J. Chamkha revised the manuscript; F. Mechighel supervised the overall work. The manuscript was written through the contribution of all authors. All authors discussed the results, reviewed, and approved the final version of the manuscript.

Acknowledgments

This work is part of a research project of the General Directorate for Scientific Research and Technological Development (DGRSDT). On the other hand, the first author would like to thank the head of the Research Unit "UR22ES12: Modeling, Optimization and Augmented Engineering, ISLAIB, University of Jendouba" for the internship carried out.

Conflict of Interest

The authors declared no potential conflicts of interest concerning the research, authorship, and publication of this article.

Funding

The authors received no financial support for the research, authorship, and publication of this article.

Data Availability Statements

The datasets generated and/or analyzed during the current study are available from the corresponding author on reasonable request.

Nomenclature

σ_e	Von-Mises stress [MPa]	T	Temperature [K]
σ_z	Axial stress [MPa]	P	Applied pressure [MPa]
\tilde{D}	Mold diameter [mm]	H	Mold height [mm]

References

- [1] Manière, C., Durand, L., Weibel, A., Estournes, C., Spark-Plasma-Sintering and Finite Element Method: From the Identification of the Sintering Parameters of a Submicronic A-Alumina Powder to the Development of Complex Shapes, Acta Materialia, 102, 2016, 169-175.
- [2] Mackie, A.J., Hatton, G.D., Hamilton, H.G.C., Dean, J.S., Goodall, R., Carbon uptake and distribution in spark plasma sintering (SPS) processed SM(Co, Fe, Cu, Zr)Z, Materials Letters, 171, 2016, 14-17.
- [3] Guillon, O., Gonzalez-Julian, J., Dargatz, B., Kessel, T., Schierning, G., Rathel, J., Herrmann, M., Field-assisted sintering technology/Spark plasma
- sintering: Mechanisms, materials, and technology developments, Advanced Engineering Materials, 16(7), 2014, 830–849.
 [4] Kumar, D.B., Babu, B.S., Jerrin, K.M.A., Joseph, N., Jiss, A., Review of spark plasma sintering process, IOP Conference Series: Materials Science and Engineering, 993, 2020, 012004.
- [5] Wang, X., Casolco, S.R., Xu, G., Garay, J.E., Finite element modeling of electric current-activated sintering: The effect of coupled electrical potential,
- [6] Mechighel, F., Pateyron, B., El Ganaoui, M., Kadja, M., Study of thermo-electrical and mechanical coupling during densification of a polycrystalline material using COMSOL, *Proceedings of the COMSOL Conference*, Hannover, Germany, 2008.
 [7] Wei, S., Zhang, Z.-H., Shen, X.-B., Wang, F.-C., Sun, M.-Y., Yang, R., Lee, S.-K., Simulation of temperature and stress distributions in functionally graded materials synthesized by a spark plasma sintering process, *Computational Materials Science*, 60, 2012, 168–175.
 [8] Yushin, D.I., Smirrov, A.V., Solis Pinargote, N., Peretyagin, P.Yu., Kuznetsov, V.A., Torrecillas, R., Spark plasma sintering of cutting plates, *Russian Pateriatrica Pateriat*
- Engineering Research, 36, 2016, 410-413.
- [9] Diatta, J., Antou, G., Pradeilles, N., Maitre, A., Numerical modeling of spark plasma sintering Discussion on densification mechanism identification and generated porosity gradients, Journal of the European Ceramic Society, 37, 2017, 4849–4860.

 [10] Bódis, E., Károly, Z., Fabrication of graded alumina by spark plasma sintering, The International Journal of Advanced Manufacturing Technology, 117,
- 2021 2835-2843 [11] Borkar, T., Banerjee, R., Influence of spark plasma sintering (SPS) processing parameters on microstructure and mechanical properties of nickel,
- Materials Science and Engineering A, 618, 2014, 176–181.

 [12] Oke, S.R., Ige, O.O., Falodun, O.E., Obadele, B.A., Shongwe, M.B., Olubambi, P.A., Optimization of process parameters for spark plasma sintering of nano structured SAF 2205 composite, *Journal of Materials Research and Technology*, 7, 2017, 126–134.
- [13] Stuer, M., Bowen, P., Zhao, Z., Spark plasma sintering of ceramics: From modeling to practice, Ceramics, 3, 2020, 476–493.
- [14] Han, C.L., Yang, X.Y., Shen, X.F., Peng, T.S., Cheng, H.F., Zhang, F.G., Zhang, J.X., Application of response surface method (RSM) to investigate the effects of process parameters on the microstructure and shear strength of TZM/graphite joints bonded by using spark plasma sintering, International



Journal of Refractory Metals and Hard Materials, 2021, 105622

[15] Khajelakzay, M., Bakhshi, S.R., Optimization of spark plasma sintering parameters of Si3N4-SiC composite using response surface methodology (RSM), Ceramics International, 43, 2017, 7060–7068.

[16] Jounaki, A., Anvari, S.Z., Utilizing response surface methodology for the microstructural examination of CeO2/GNP composite coating applied via air plasma spraying and post-treated with spark plasma sintering, Heliyon, 10, 2024, e29411.

[17] Oketola, A., Jamiru, T., Ogunbiyi, O., Rominiyi, A.L., Smith, S., Adedayo, O.D., Process parametric optimization of spark plasma sintered Ni-Cr-ZrO2 composites using response surface methodology (RSM), International Journal of Lightweight Materials and Manufacture, 7, 2023, 14–24.

[18] Ogunbiyi, O., Jamiru, T., Sadiku, R., Adesina, O., Olajide, J.L., Beneke, L., Optimization of spark plasma sintering parameters of Inconel 738LC alloy using response surface methodology (RSM), International Journal of Lightweight Materials and Manufacture, 3, 2019, 177–188.

[19] Ujah, C.O., Popoola, A.P.I., Popoola, O.M., Aigbodion, V.S., Optimisation of spark plasma sintering parameters of Al-CNTs-Nb nano-composite using Taguchi Design of Experiment, The International Journal of Advanced Manufacturing Technology, 100, 2019, 1563–1573.
[20] Kumar, N., Soren, S., Prasad, R., Singh, Y., Nautiyal, H., Sharma, A., Tiang, S.S., Lim, W.H., Optimization of sintering process parameters by Taguchi

method for developing Al-CNT-reinforced powder composites, Crystals, 13, 2023, 1352.

[21] Ali, M., Hussein, M.A., Al-Aqeeli, N., Optimization of spark plasma sintering parameters using the Taguchi method for developing Mg-based composites, Advanced Manufacturing for Biomaterials and Biological Materials, 72(3), 2020, 1186-1194.

[22] Nasri, W., Djebali, R., Chamkha, A.J., Bezazi, A., Mechighel, F., Reis, P., Driss, Z., Thermal behavior of mesoporous aramid fiber reinforced silica aerogel composite for thermal insulation applications: Microscale modeling, Journal of Applied and Computational Mechanics, 10(1), 2024, 140–151.

[23] Ferhi, M., Abidi, S., Djebali, R., Mebarek-Oudina, F., Assessment of micro-scale heat exchangers efficiency using lattice Boltzmann method and design of experiments, Energy and Built Environment, 5(6), 2023, 840-852.

[24] Zhang, W., Chen, C., Pan, Z., Zheng, Z., Vacuum and infrared-assisted hot air impingement drying for improving the processing performance and quality of Poria cocos (Schw.) Wolf cubes, Foods, 10, 2021, 992.

[25] Halson, S.L., Shaw, G., Versey, N., Miller, D.J., Sargent, C., Roach, G.D., Nyman, L., Carter, J.M., Baar, K., Optimisation and validation of a nutritional intervention to enhance sleep quality and quantity, Nutrients, 12, 2020, 2579.

[26] Campbell, K.T., Wysoczynski, K., Hadley, D.J., Silva, E.A., Computational-based design of hydrogels with predictable mesh properties, ACS Biomaterials Science & Engineering, 6(1), 2020, 308-319.

[27] Kriba, A., Mechighel, F., Three-dimensional numerical study of the behavior of thermoelectric and mechanical coupling during spark plasma sintering of a poly-crystalline material, Archive of Mechanical Engineering, 70(4), 2023, 497–529.
[28] Cincotti, A., Locci, A.M., Orrù, R., Cao, G., Modeling of SPS apparatus: Temperature, current and strain distribution with no powders, AIChE Journal,

[29] Muñoz, S., Anselmi-Tamburini, U., Temperature and stress fields evolution during spark plasma sintering processes, Journal of Materials Science, 45, 2010, 6528-6539.

ORCID iD

Abdelmalek KRIBA https://orcid.org/0009-0009-4219-5217 Farid MECHIGHEL https://orcid.org/0000-0002-4726-7613 Ridha DJEBALI https://orcid.org/0000-0002-1017-3410 Ali J. CHAMKHA https://orcid.org/0000-0002-8335-3121



© 2025 Shahid Chamran University of Ahvaz, Ahvaz, Iran. This article is an open access article distributed under the terms and conditions of the Creative Commons Attribution-NonCommercial 4.0 International (CC BY-NC 4.0 license) (http://creativecommons.org/licenses/by-nc/4.0/).

How to cite this article: KRIBA A., et al., DoE Optimization of Applied Pressure and Mold Size in Manufacturing Homogeneous Samples by SPS Process under 1000A Current, J. Appl. Comput. Mech., xx(x), 2025, https://doi.org/10.22055/jacm.2025.48063.4953

Publisher's Note Shahid Chamran University of Ahvaz remains neutral with regard to jurisdictional claims in published maps and institutional affiliations.

